electron helicity limits the ratios C_A'/C_A and C_T/C_A, each under the appropriate assumption regarding the other, is apparent from Eqs. (11) and (12). Sequentially assigning the deviation from $\mathcal{H}=-v/c$ permitted by an experimental uncertainty of 1 standard deviation to a departure from the two-component neutrino theory and then to an admixture of the tensor interaction limits the ratio C_A'/C_A to values between 0.90 and 1.11 and the ratio $C_T/C_A<0.0029$.

Combining these results with the results of other measurements at higher energies,[6] the v/c dependence of the helicity required by the two-component neutrino hypothesis has now been verified from $v/c=0.4$ to 0.9 for allowed Gamow-Teller transitions. The present level of accuracy precludes the observation of small corrections due to higher-order transitions, finite nuclear size, and screening by atomic electrons.[29] Of these, the latter is expected to produce the largest effect: a reduction of the polarization by a fraction of 1% at the higher momenta and by 2% at $v/c=0.41$. It would be difficult to extend these measurements to lower energies, or sufficiently improve the accuracy with the present techniques so that a significant improvement in the determination of the coupling constant could be obtained. We point out again, however, that the helicities for the Fermi transitions are presently only poorly determined.

[29] W. Bühring, Nucl. Phys. 40, (1963); 61, 110 (1965).

ACKNOWLEDGMENTS

We wish to thank Professor S. R. Lin and Professor R. L. Gluckstern for the calculations of the asymmetry function, cross sections, and multiple scattering effects as well as many helpful discussions. We gratefully acknowledge the assistance of Professor K. S. R. Sastry and Richard Treffers. Irwin Gruverman of New England Nuclear Corporation prepared the sources. We wish to thank Professor V. W. Hughes for his continued interest and support.

PHYSICAL REVIEW D VOLUME 2, NUMBER 1 1 JULY 1970

Photoproduction of Electron-Positron Pairs at 2.3 and 5.6 GeV†*

J. Tenenbaum,‡ A. M. Eisner,§ G. J. Feldman,§ W. Lockeretz, F. M. Pipkin, and J. K. Randolph‖
Cyclotron Laboratory, Harvard University, Cambridge, Massachusetts 02138
(Received 27 February 1970)

We have measured the photoproduction of electron-positron pairs from carbon using an improved version of the Harvard pair spectrometer. The bending magnet and two half-quadrupole magnets were retained. For each half-quadrupole, a tungsten collimator was added at the entrance, a portion of the lead obstacle was removed, and a defining counter was added at the midpoint. Faster counting electronics and an on-line computer were employed. Pairs were detected in an invariant-mass range of 97–445 MeV. The results are in agreement with the predictions of quantum electrodynamics and may be parametrized as $R=(1.09\pm0.07)\times[1+(31.6_{-41.2}^{+31.2})\times10^{-8}Q_M^2]$. Here R is the ratio of experiment to theory, and Q_M^2 is the electron-pair mass squared (GeV$^2/c^4$). The errors include both statistical and systematic effects. In the course of this work, we have also derived an accurate approximation for the electron-pair cross section.

I. INTRODUCTION

The modern formulation of quantum electrodynamics (QED) resulted from the work of Feynman, Schwinger, and Tomonaga. The Lamb shift in hydrogen and the radiative correction to the gryomagnetic ratio of the electron gave the first confirmation of the theory. These radiative effects are sensitive to the high-energy behavior of the virtual particles in the higher-order Feynman diagrams. Since the contribution of the higher-order diagrams is small, the measurements must be made to high precision in order to check the theory. The current situation for low-energy tests of QED has been reviewed by Brodsky.[1] At present the experimental values for the Lamb shift and the gyromagnetic ratio of the electron do not agree with the theoretical values. The most sensitive test, the gyromagnetic ratio of the muon, gives agreement between experiment and theory.

During the past ten years, high-energy experiments have been used to give a different kind of test of QED. The precision is less than that of atomic physics experiments, but the experiments are more directly sensitive to the high-energy behavior. Drell[2] suggested that a breakdown of QED might occur in three different

† Work supported by the U. S. Atomic Energy Commission under Contract No. AT(30-1)2752.

* Paper based in part on a thesis submitted by one of the authors (JT) to Harvard University in partial fulfillment of the requirements for the Doctor of Philosophy in Physics.

‡ Present address: Stanford Linear Accelerator Center, Stanford, Calif.

§ National Science Foundation Graduate Fellow.

‖ Present address: Randall Laboratory of Physics, University of Michigan, Ann Arbor, Mich.

[1] S. J. Brodsky, in *International Symposium on Electron and Photon Interactions at High Energies, Liverpool, England, 1969*, edited by D. W. Broben (Daresbury Nuclear Physics Laboratory, Daresbury, Lancashire, England, 1970), p. 3.

[2] S. D. Drell, Ann. Phys. (N. Y.) 4, 75 (1958).

places: the lepton propagator, the photon propagator, or the lepton vertex. Different experiments are sensitive to one or more of these items. Lepton-lepton scattering is sensitive to the photon propagator in the spacelike region, lepton bremsstrahlung to the photon propagator in the timelike region, and lepton pair production to the lepton propagator in the spacelike region.

All three types of experiments have now been performed.[3–5] With the exception of wide-angle lepton pair production, all of the experiments have indicated no deviation between experiment and theory. A single-arm experiment detecting only one member of the electron pair gave satisfactory agreement between theory and experiment.[6] The first Harvard high-energy measurement of wide-angle electron pairs indicated a substantial excess of electron pairs over that predicted by theory.[7] A corresponding muon-pair experiment indicated a small energy-dependent deficit of muon pairs.[8] A Cornell experiment gave an ambiguous result.[9] More recent measurements of both electron and muon pairs have given good agreement with QED.[10–13]

This paper reports a new measurement at the Cambridge Electron Accelerator of the photoproduction from carbon of symmetric electron-positron pairs. The experiment used an improved version of the previous Harvard apparatus. The purpose of the experiment was to confirm or disprove the deviation between theory and experiment observed in the first Harvard electron-pair experiment. Data were taken at electron half-angles of 3.4° and 5.8°, and electron momenta of 0.9 and 2.25 GeV/c. The results do not reproduce the results of the first Harvard experiment and are in agreement with the predictions of QED.

This paper treats in sequence the theory behind the experiment, the apparatus, the experimental problems and methods, the rate calculations and corrections, and the results and conclusions. Appendices deal with the reduction of the electron-pair cross section, a discussion of the first Harvard electron-pair experiment, and the calculation of the corrections due to multiple scattering.

II. THEORY

A. Electron-Pair Experiments

Electron pair production is represented by the two Feynman diagrams shown in Figs. 1(a) and 1(b). It can be used to study the behavior of the theory when the mass of the virtual fermion, Q_F, is large. Table I summarizes the definitions of important quantities used in this paper. In this table and throughout the rest of this paper we shall whenever possible neglect the contributions due to the mass of the electron.

The electron propagator is defined differently for the two diagrams. For the diagram in Fig. 1(a),

$$Q_F^2 = -2k\cdot p_+. \tag{1}$$

For the diagram in Fig. 1(b),

$$Q_F^2 = -2k\cdot p_-. \tag{2}$$

Here k, p_+, and p_- are the four-vector momenta of the photon, positron, and electron, respectively. Symmetric experiments have comparable values of Q_F^2 in both diagrams. To avoid ambiguity, especially in comparing with asymmetric experiments, we will deal with the electron-pair mass,

$$Q_M^2 = 2p_+\cdot p_-. \tag{3}$$

For symmetric experiments,

$$Q_M^2 \approx -2Q_F^2. \tag{4}$$

There are two problems in interpreting the electron-pair experiment as a test of QED. First, there are the virtual Compton diagrams shown in Figs. 1(c) and 1(d). The virtual fermion propagator is absent in these diagrams. Second, the coupling of the photon to the nucleus may be affected by a form factor at large values of q^2, the momentum transfer to the nucleus. Both problems are reduced if we limit ourselves to symmetric electron pairs.

The electrodynamic amplitude for pair production may be written

$$M = M_{\rm BH} + M_{\rm C}, \tag{5}$$

where $M_{\rm BH}$ is the amplitude from the Bethe-Heitler diagrams and $M_{\rm C}$ is the amplitude from the Compton diagrams. In the cross section the interference term involves three photons coupled to electron lines. Since the photon has odd charge-conjugation parity, the interference term will vanish for any symmetric con-

[3] For electron-electron scattering, see W. C. Barber, B. Gittleman, G. K. O'Neill, and B. Richter, Phys. Rev. Letters **16**, 1127 (1966).

[4] For wide-angle electron bremsstrahlung, see R. H. Siemann, W. W. Ash, K. Berkelman, D. L. Hartill, C. A. Lichtenstein, and R. M. Littauer, Phys. Rev. Letters **22**, 421 (1969).

[5] For wide-angle muon bremsstrahlung see A. D. Liberman, C. M. Hoffman, E. Engles, Jr., D. C. Imrie, P. G. Innocenti, R. Wilson, C. Zajde, W. A. Blanpied, D. G. Stairs, and D. Drickey, Phys. Rev. Letters **22**, 663 (1969).

[6] B. Richter, Phys. Rev. Letters **1**, 114 (1958).

[7] R. B. Blumenthal, D. C. Ehn, W. L. Faissler, P. M. Joseph, L. J. Lanzerotti, F. M. Pipkin, and D. G. Stairs, Phys. Rev. **144**, 1199 (1966).

[8] P. L. Rothwell, R. C. Chase, D. R. Earles, M. Gettner, G. Glass, G. Lutz, E. von Goeler, and R. Weinstein, Phys. Rev. Letters **23**, 1521 (1969).

[9] E. Eisenhandler, J. Feigenbaum, N. Mistry, P. Mostek, D. Rust, A. Silverman, C. Sinclair, and R. Talman, Phys. Rev. Letters **18**, 425 (1967).

[10] J. G. Asbury, W. K. Bertram, U. Becker, P. Joos, M. Rohde, A. J. S. Smith, S. Friedlander, C. L. Jordan, and S. C. C. Ting, Phys. Rev. **161**, 1344 (1967); H. Alvensleben, U. Becker, W. K. Bertram, M. Binkley, K. Cohen, C. L. Jordan, T. M. Knasel, R. Marshall, D. J. Quinn, M. Rohde, G. H. Sanders, and S. C. C. Ting, Phys. Rev. Letters **21**, 1501 (1968).

[11] K. J. Cohen, S. Homma, D. Luckey, and L. S. Osborne, Phys. Rev. **173**, 1339 (1968).

[12] P. J. Biggs, D. W. Braben, R. W. Clifft, E. Gabathuler, P. Kitching, and R. E. Rand, Phys. Rev. Letters **23**, 927 (1969).

[13] S. Hayes, R. Imlay, P. M. Joseph, A. S. Keizer, J. Knowles, and P. C. Stein, Phys. Rev. Letters **22**, 1134 (1969).

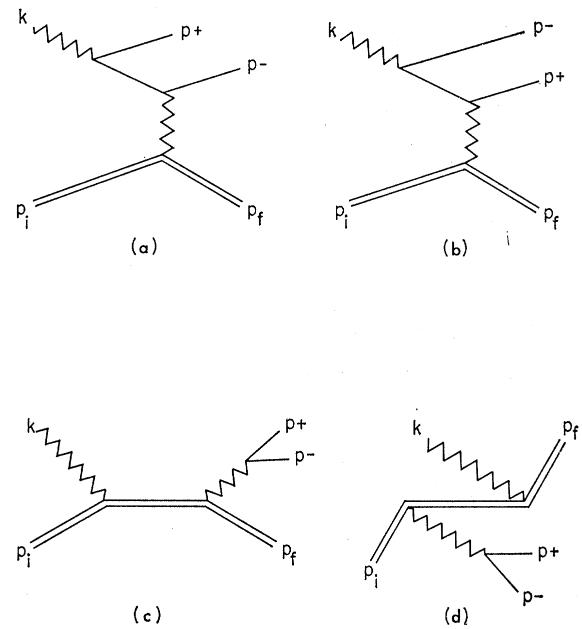

FIG. 1. Feynman diagrams for the dominant processes which contribute to the photoproduction of wide-angle electron pairs. Diagrams (a) and (b) are the Bethe-Heitler diagrams which are of interest in a test of QED. Diagrams (c) and (d) are the background Compton diagrams which do not test QED.

figuration of the apparatus.[14] As part of a concurrent experiment searching for Compton terms, we have shown that the interference term is small in the electron-pair mass range less than 500 MeV/c^2.[15]

The uncertainties due to the nuclear form factor are reduced by using a symmetric configuration; this choice minimizes the momentum transfer to the nucleus. Carbon was chosen over hydrogen to increase the counting rate ($\sim Z^2$). The carbon nucleus has a simple, spin-0 ground state. The carbon form factor has been studied in separate experiments.[16–19] The essential conclusion was that the cross section is well described by a sum rule given by Drell and Schwartz.[20] For the range of nuclear four-momentum transfers, q^2, in this experiment the elastic form factor is a factor of 1000 greater than all other contributions. In our calculations we have used the following expression ($q^2<0$):

$$Z^2W_2=[G_{Ep}(q^2)][Z+e^{+x}(30+16x+8x^2/9)-(Zq^2/2AM_p^2)+\tfrac{2}{3}(Z/AM_p)\langle T\rangle-(q^2/4M_p^2)(Z\mu_p^2+N\mu_n^2)], \quad (6)$$

TABLE I. Definition of variables.

$p_+=(E_+,\mathbf{p}_+)$,	four-momentum of positron
$p_-=(E_-,\mathbf{p}_-)$,	four-momentum of electron
$k=(k,\mathbf{k})$,	four-momentum of incident photon
$p_i=(E_i,\mathbf{p}_i)$,	four-momentum of initial nucleus
$p_f=(E_i,\mathbf{p}_f)$,	four-momentum of final nuclear state
$q=k-p_+-p_-$,	four-momentum transfer to nucleus
$Q_M^2\cong 2p_+\cdot p_-$,	mass squared of the electron-positron final state
$Q_F^2\cong -2k\cdot p_+$ or $-2k\cdot p_-$,	mass of the virtual fermion
$\theta_+=$	angle between $\mathbf{p}_+$ and $\mathbf{k}$
$\theta_-=$	angle between $\mathbf{p}_-$ and $\mathbf{k}$
$\varphi=$	angle between normal to $\mathbf{k},\mathbf{p}_+$ and $\mathbf{k},\mathbf{p}_-$ planes
$M_i^2=p_i\cdot p_i$,	mass squared of initial nucleus
$M_f^2=p_f\cdot p_f$,	mass squared of final nuclear state
$M=$	carbon mass ($=M_i=M_f$ for elastic scattering)
$m=$	electron mass
$\theta=\frac{1}{2}(\theta_++\theta_-)$,	average angle
$E=\frac{1}{2}(E_++E_-)$,	average energy
$a=(\theta_+-\theta_-)/(\theta_++\theta_-)$,	angular asymmetry
$e=(E_+-E_-)/(E_++E_-)$,	energy asymmetry
$u^2=(a+e)^2+\frac{1}{4}\varphi^2$,	pair asymmetry parameter
$f=f(k,k_x)$,	deviation of the bremsstrahlung spectrum from a $1/k$ behavior
$k_x=$	end-point energy of the bremsstrahlung spectrum

where

$Z=$ atomic number of the target nucleus ($Z=6$),
$A=$ atomic weight of the target nucleus ($A=12$),
$N=$ neutron number of the target nucleus ($N=6$),
$W_2=$ the total form factor,
$G_{Ep}(q^2)=$ the form factor for a free proton,
$x=\frac{1}{2}q^2a^2$,
$a=1.637$ F,

and

$\langle T\rangle=20$ MeV.

This is the result of Ref. 18 with the assumptions that

$$2\tan^2(\tfrac{1}{2}\theta)W_1\ll W_2$$

and

$$2\tan^2(\tfrac{1}{2}\theta)\ll 1.$$

For $G_{Ep}(q^2)$ we used the standard dipole fit[21]:

$$G_{Ep}(q^2)=1/(1-q^2/0.71)^2. \quad (7)$$

B. Electron-Pair Cross Sections

The lepton-pair cross section was first calculated by Bethe and Heitler (BH).[22] They treated the nucleus as a known external potential and ignored form factors and nuclear recoil. After pair production was suggested as a

[14] J. D. Bjorken, S. D. Drell, and S. C. Frautschi, Phys. Rev. **112**, 1409 (1958).
[15] J. K. Randolph, thesis, Harvard University, 1965 (unpublished).
[16] J. Fregeau, Phys. Rev. **104**, 225 (1956).
[17] H. Crannell, Phys. Rev. **148**, 1107 (1966).
[18] W. L. Faissler, F. M. Pipkin, and K. C. Stanfield, Phys. Rev. Letters **19**, 1202 (1967).
[19] K. C. Stanfield, thesis, Harvard University, 1969 (unpublished).
[20] S. D. Drell and C. L. Schwartz, Phys. Rev. **112**, 568 (1958).
[21] For a discussion of nucleon form factors, see J. G. Rutherglen, in *International Symposium on Electron and Photon Interactions at High Energies, Liverpool, England, 1969*, edited by D. W. Braben (Daresbury Nuclear Physics Laboratory, Daresbury, Lancashire, England, 1970), p. 163.
[22] H. A. Bethe and W. Heitler, Proc. Roy. Soc. (London) **A146**, 83 (1934).

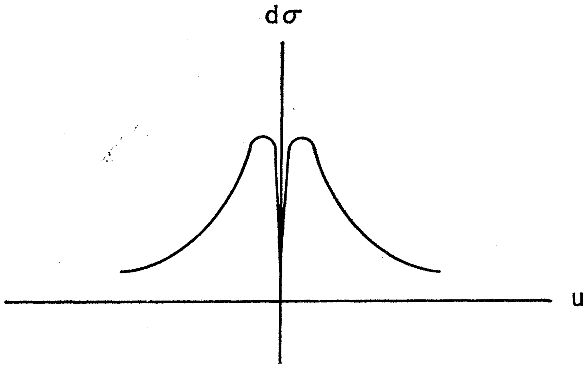

FIG. 2. Shape of the pair production cross section as a function of the asymmetry parameter u.

test of QED, Bjorken, Drell, and Frautschi (BDF) calculated the cross section allowing for nuclear recoil and an elastic form factor.[14] Later, Drell and Walecka (DW) extended the calculations to elastic and inelastic form factors and retained all lepton mass terms.[23] For the energies in the current experiment, the electron mass may be neglected.

The BDF and DW formulas for the electron-positron pair production cross section for a bremsstrahlung beam incident on a carbon target may be written

$$d\sigma_{\mathrm{BDF,DW}}=\frac{\alpha^3}{4\pi^2}\frac{d^3p_+}{E_+}\frac{d^3p_-}{E_-}\frac{f}{k}\frac{1}{q^4}\frac{2B}{k\cdot p_+k\cdot p_-}\frac{F^2}{k}, \tag{8}$$

where F is the carbon form factor, f describes the bremsstrahlung spectrum, and

$$B=-[(k\cdot p_+)^2+(k\cdot p_-)^2+q^2(p_+\cdot p_-)+q^2(E_+{}^2+E_-{}^2)]. \tag{9}$$

The cross section is per equivalent quantum. A derivation of this form and some useful approximations to the four-vector products are given in Appendix A. The photon spectrum is given by $f(k,k_x)/k$, where k is the photon energy and k_x is the bremsstrahlung end-point energy (see Sec. V E).

Two items should be noted about the cross section. First, there is a deep dip at exact symmetry. This dip is difficult to resolve experimentally and occurs in a number of related electrodynamic processes.[24] Second, because of large cancellations, care must be used in evaluating the cross section numerically. This is discussed further in Appendix A.

One of us (JT) has derived an approximate form of the cross section which eliminates the cancellations. It is

$$\frac{d\sigma}{dE_+d\Omega_+dE_-d\Omega_-}=\frac{\alpha^3}{4\pi^2}\frac{fF^2}{E^4\theta^6}\frac{u^2+\frac{1}{4}\theta^4}{4(u^2+\frac{1}{4}\theta^2)^2}, \tag{10}$$

where

$$E=\tfrac{1}{2}(E_++E_-), \tag{11}$$

$$\theta=\tfrac{1}{2}(\theta_++\theta_-), \tag{12}$$

$$e=(E_+-E_-)/(E_++E_-), \tag{13}$$

$$a=(\theta_+-\theta_-)/(\theta_++\theta_-), \tag{14}$$

$$u^2=(a+e)^2+\tfrac{1}{4}\varphi^2, \tag{15}$$

and φ is the angle between the normal to the $\mathbf{k}$, $\mathbf{p}_+$ and $\mathbf{k}$, $\mathbf{p}_-$ planes (symmetry is $\varphi\approx 0$). The term $\frac{1}{4}\theta^4$ is not important but is retained to show the behavior at exact symmetry. This approximate form duplicates the results of either the BDF or DW expression to better than 1% for values of a or e up to 0.1. It shows the existence of a deep dip at symmetry ($u=0$) and is an expansion about symmetry in a, e, and φ and about the forward direction in θ. The shape of the function is shown in Fig. 2; the relative heights at the peak and dip are $1/\theta^2$ and 1.

For a spectrometer with a constant fractional momentum acceptance $\Delta E/E$ and small angular acceptance $\Delta\Omega$ we may derive a scaling law from the approximate form of the cross section. The yield per equivalent quantum, Y, is given by

$$Y\propto\frac{d\sigma}{(d\Omega)^2(dE)^2}(\Delta E)^2(\Delta\Omega)^2\propto\frac{\alpha^3}{4\pi^2}\frac{fF^2}{E^2\theta^6}\frac{u^2}{(u^2+\frac{1}{4}\theta^2)^2}. \tag{16}$$

Y depends on energy as $1/E^2$. No other quantity in this expression depends on the absolute energy through second order. The variable e (in u^2) depends only on the relative energy within the acceptance. Hence, aside from multiple scattering and radiative corrections, the yields per equivalent quantum at a fixed angle vary as $1/E^2$. QED can thus be tested without relying on the Monte Carlo integration (see Sec. V H).

In Appendix A it is shown that

$$q^2\approx-4E^2\theta^2(u^2+\tfrac{1}{4}\theta^2). \tag{17}$$

This formula can be used to rewrite the cross section in the form

$$d\sigma=\frac{\alpha^3}{4\pi^2}\frac{d^3p_+}{E_+}\frac{d^3p_-}{E_-}fF^2\frac{1}{q^4}\frac{-[q^2-(q^2)_{\mathrm{min}}]}{k\cdot p_+k\cdot p_-}. \tag{18}$$

The $1/q^4$ factor comes from the photon propagator characteristic of low-q^2 potential scattering. A 5% experiment is not sensitive to any of the corrections calculated by BDF or DW. The $1/q^4$ factor contributes a major portion of the energy and angle dependence; very little of the observed E or θ dependence is due to the electron propagator.

C. Radiative Corrections

The normal operating conditions were $E_++E_-=k=0.8k_x$. Such a procedure made the result insensitive

[23] S. D. Drell and J. D. Walecka, Ann. Phys. (N. Y.) **28**, 18 (1964).

[24] Consequently, the cross section at exact symmetry is both qualitatively and quantitatively different from the observed cross section. See G. R. Henry, Phys. Rev. **153**, 1649 (1967).

to the detailed shape of $f(k,k_x)$. The main disadvantage to this choice of running conditions is that processes of the form

$$\gamma(0.9k_x) \rightarrow e^+(0.5k_x)+e^-(0.4k_x) \\ \searrow \\ e^+(0.4k_x)+\gamma(0.1k_x) \qquad (19)$$

are possible. The indicated bremsstrahlung may occur either as a higher-order correction or as additional bremsstrahlung in the target. We will refer to these processes as real-photon and target-bremsstrahlung radiative corrections, respectively. Another higher-order correction is illustrated by the Feynman diagrams in Fig. 3. This process will be referred to as the virtual-photon radiative correction.

The first calculations of the radiative corrections were made by BDF.[14] They kept only the leading logarithmic terms in the virtual-photon corrections, and their calculation of the real-photon radiative correction was not consistent. Huld has subsequently made a complete calculation of the radiative corrections.[25] Huld's result for the virtual-photon correction is

$$d\sigma_{\mathrm{virt}}=\frac{\alpha}{2\pi}\left[3\ln\left(\frac{\beta}{m^2}\right)+\tfrac{4}{3}\ln\left(\frac{-q^2}{m^2}\right)-\pi^2 -\frac{65}{9}+5\ln^2 2-2\ln 2+2\right]d\sigma_{\mathrm{BH}}\,, \qquad (20)$$

where

$$\beta=k\cdot p_+ + k\cdot p_-\,. \qquad (21)$$

For $E_+=E_-=2.5$ GeV, $\theta_+=\theta_-=5°$, the correction to the cross section is $(4.00\pm0.25)\%$. The real-photon corrections were evaluated in the peaking approximation and they are given by the expression

$$d\sigma_{\mathrm{real}}=-\frac{\alpha}{\pi}\left[\ln\left(\frac{Q_M{}^2}{m^2}\right)-1\right]\ln\left(\frac{E_+E_-}{(\Delta E)^2}\right)d\sigma_{\mathrm{BH}} +I(p_+,p_-,\Delta E)\,, \qquad (22)$$

with $\Delta E=k_x-E_+-E_-$, $Q_M{}^2=(p_++p_-)^2$. The expression for $I(p_+,p_-,\Delta E)$ is a complicated function containing portions multiplying $d\sigma_{\mathrm{BH}}$ and $d\sigma_{\mathrm{BH}}$ evaluated at symmetry. It is given explicitly in Eq. (C1) of Huld's paper. The numerical value of the correction for $E_+=E_-=2.5$ GeV, $\theta_+=\theta_-=5°$, is $(-16\pm2)\%$.

The target-bremsstrahlung correction is related to the real-photon correction in a simple way. The real-photon correction may be considered to be the bremsstrahlung from a target of length

$$t_{\mathrm{eff}}=\frac{3}{4}\frac{\alpha}{\pi}\left[\ln\left(\frac{Q_M{}^2}{m^2}\right)-1\right]. \qquad (23)$$

Hence for the target bremsstrahlung we need only apply the real-photon correction with $t_{\mathrm{eff}}=\frac{1}{2}t_{\mathrm{tgt}}$. Here t_{tgt} is the length of the target in radiation lengths and the factor of $\frac{1}{2}$ indicates that the average pair is produced at the midpoint of the target. The target bremsstrahlung may also be treated in the same way as the arm bremsstrahlung (see Sec. V G). The cross sections as corrected by these two methods agree within 2%.

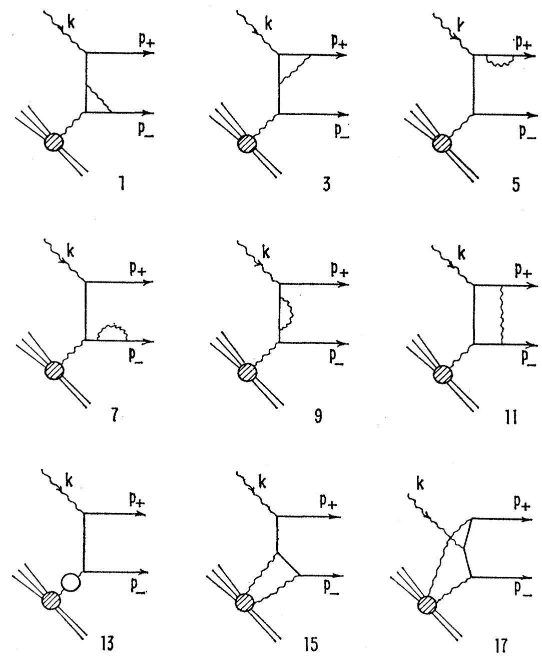

FIG. 3. Feynman diagrams for the virtual-photon correction. Each even-numbered diagram (not shown) can be obtained by exchanging p_+ and p_- on the preceding odd-numbered diagram.

III. EXPERIMENTAL APPARATUS

A. Introduction

The apparatus for this experiment was an improved version of the Harvard pair spectrometer used in the first electron-pair experiment.[26] The basic scheme of the bending magnet followed by a single quadrupole spectrometer was retained. The major changes were the addition of a tungsten collimator between the bending magnet and the quadrupole magnet, the removal of the downstream portion of the lead obstacle, the subdivision of the momentum and angle acceptance by hodoscopes, and the extension of the image plate of the half-quadrupole magnets. The counting electronics were replaced by 100-MHz circuitry. An on-line computer was used to record hodoscope and diagnostic information. Figure 4 shows an over-all view of the apparatus; Fig. 5 shows the layout of one of the spectrometer arms. In Appendix B we discuss the relation of the apparatus to that of the first Harvard experiment[7] in greater detail.

[25] B. Huld, Phys. Rev. 168, 1782 (1968).

[26] For additional details concerning the apparatus, see J. Tenenbaum, thesis, Harvard University, 1969 (unpublished).

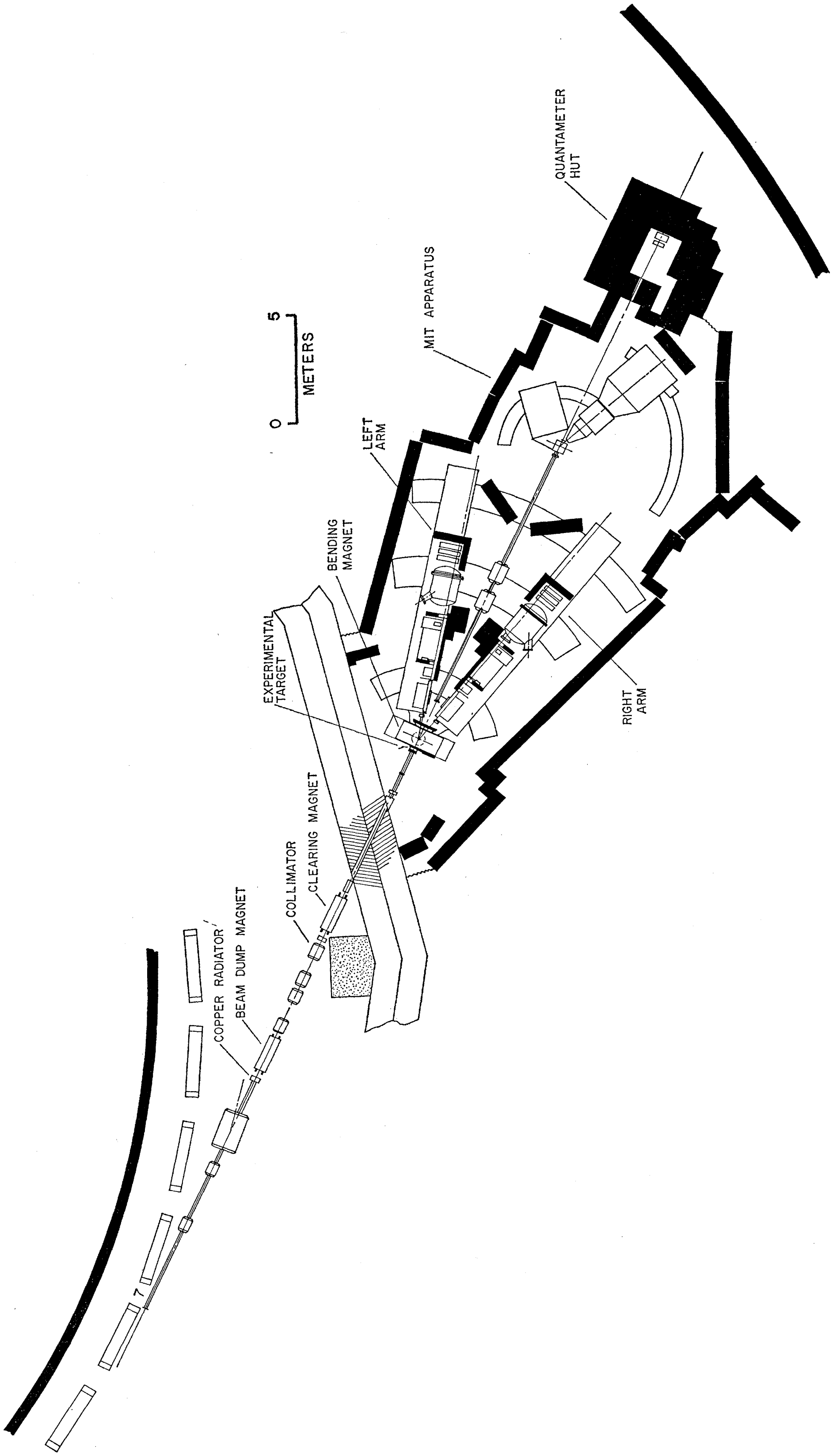

FIG. 4. Schematic diagram of the apparatus showing its relationship to the synchrotron and the external electron beam.

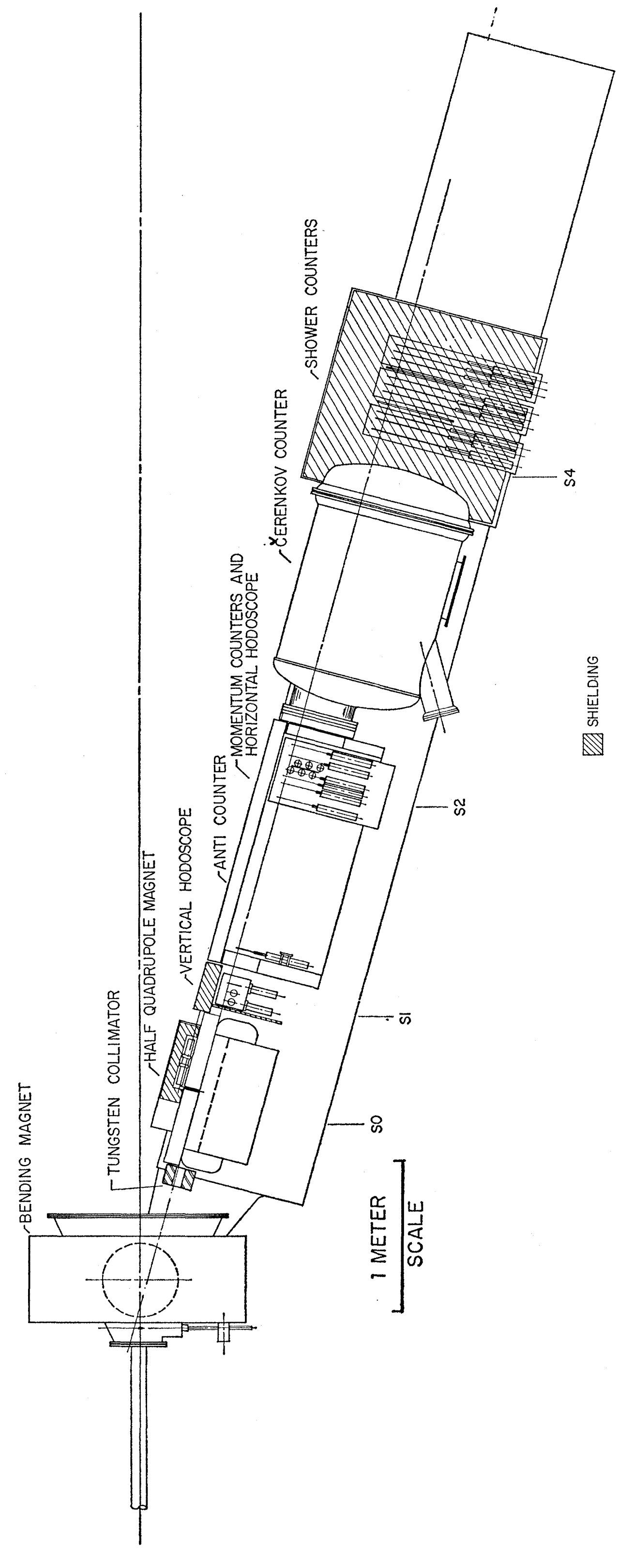

FIG. 5. Schematic diagram of the right arm showing the relative location of the magnets and counters.

B. Photon Beam

Photons were obtained by bremsstrahlung from a radiator in an external electron beam 58 ft upstream of the experimental target. The external electron beam made it possible to use electron scattering to test the spectrometer. Copper radiators of 0.1 and 0.2 radiation lengths (r.l.) were used to produce a photon beam. A magnet bent the electron beam downwards into a beam dump located in the accelerator target area.

The photon beam passed through a tungsten collimator followed by a magnet to remove charged particles. The beam then emerged through the accelerator shielding wall into the experimental hall. The entire external beam run was part of the synchrotron vacuum system. The radiator and collimator operated within this vacuum. The photon beam was collimated to produce a spot at the target 0.75 in. high by 0.75 or 1.00 in. wide. Within this collimated spot the photon flux was checked for uniformity using x-ray film. The film was measured with a densitometer and gave no indication of significant nonuniformities.

The experimental target was a block of 99.93% pure CCT grade carbon. The bulk of the electron-pair data was taken with a 0.5-in. target, 2.157 g/cm^2 thick. The target was located in a vacuum chamber just upstream of the bending magnet and could be remotely removed from the beam. Synchrotron vacuum was used up to an 0.0015-in. aluminum isolation window 8 in. upstream of the target. The bending magnet was provided with an aluminum vacuum vessel kept at a pressure of 10 m Torr. The downstream end of this vessel was a 0.002-in.-thick stainless steel window. After a 4-ft gap the beam remained in a vacuum pipe to a point downstream of the spectrometer arms.

C. Half-Quadrupole Spectrometers

To permit easy change of angle the spectrometers were mounted on movable arms. With the bending magnet on, the apparent position of the target was several inches away from its real position. To allow for the offset the nominal centerline of the spectrometer pointed at the virtual target. During electron scattering runs, the bending magnet was not used and the spectrometer arms pointed directly to the real target. To permit this pivot motion the spectrometer arms used an air suspension system rather than wheels. Three magnets were used in the spectrometer system. A 32-in.-diam circular bending magnet with a 5-in. gap bent each member of the pair 9.35° outward. Each spectrometer arm contained a 6-in.-radius half-quadrupole magnet made from a standard quadrupole split along a symmetry plane. The two missing poles were replaced by an iron image plate. The image plates were 64 in. long and extended 8 in. past each end of the 48-in.-long quadrupoles.

Each quadrupole focused vertically and defocused horizontally. The aperture between 3 in. above and 3 in. below the median plane was filled with lead for the first

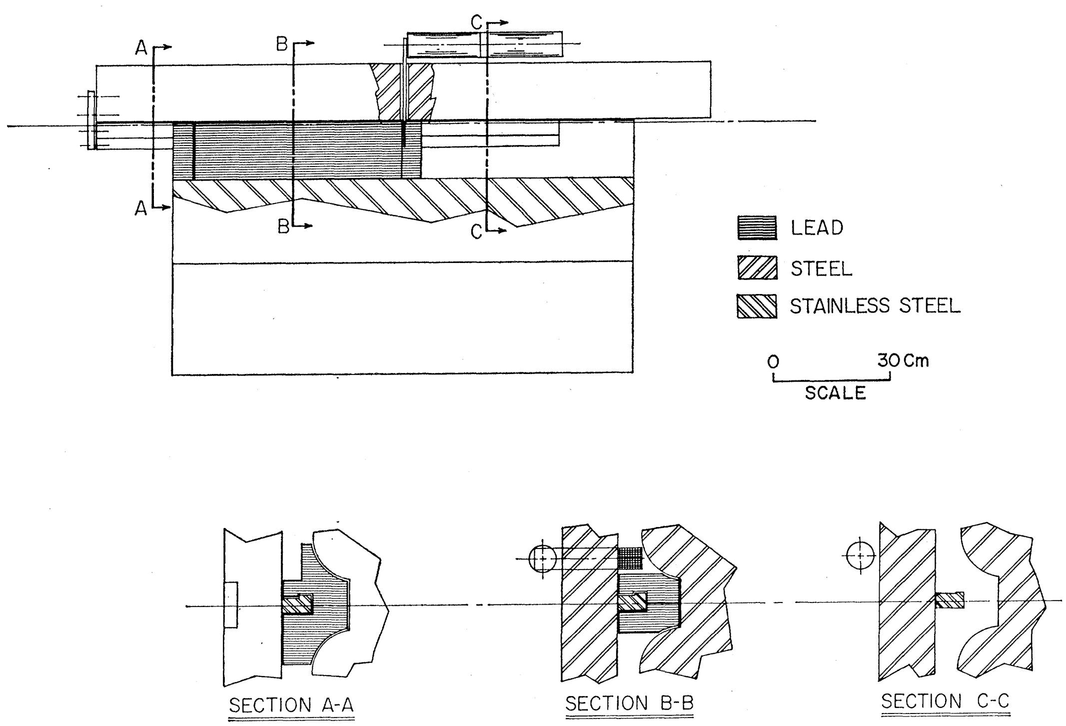

FIG. 6. Cross-sectional view of the right-arm half-quadrupole magnet showing the position of counter S0, the front lead mask, and the construction and support of the plug in the center of the quadrupole.

26 in. along the magnet. Figure 6 shows several cross sections through the quadrupoles. This lead obstacle allowed the quadrupole to function as a momentum-determining element; particles of a specific momentum came to a focus independent of the initial vertical angle. Only one quadrant of each half-quadrupole was used. The edge of the aperture was located 1.25 in. from the plane containing the photon beam. The first block of the quadrupole obstacle was a 2-in.-thick lead mask with an opening sufficiently large that it did not define the acceptance. The mask served to stop particles which were substantially off in momentum or angle. This decreased the background rates in the first few scintillation counters. The mask was not sufficient to limit the instantaneous rates in the counter at the midpoint of the quadrupole. A tungsten alloy ("Hevimet") collimator was placed between the bending magnet and the quadrupole. The collimator consisted of a 2.0-by-2.2-in. tunnel through an 8.0-in. cube. The location of the collimator is shown in Fig. 5. The tunnel edges were located 0.200 in. away from the nearest accepted trajectory. The collimator significantly attenuated electromagnetic showers produced by 0° pairs. Because of the ±0.375-in. height of the photon beam, these pairs extended above and below the median plane of the bending magnet to within 0.875 in. of the aperture at the entrance to the quadrupoles.

D. Scintillation Counters and Aperture Definition

The trigger counters were designed to provide a scintillation-counter-defined aperture. Less than 5% of the otherwise valid rays were stopped by the interior of the quadrupoles. Figure 7 shows the counter layout. In the basic fourfold coincidence, the counter at the midpoint of the quadrupole, S0, defined the vertical and horizontal acceptance. S0 was 2.42 in. high by 2.18 in. wide. The vertical angle hodoscope and S1 followed the quadrupole at a distance (S1) of 23.25 in. The momentum defining counter, S2, was 1.425 in. high at a distance of 108 in. from the rear of the quadrupole. Surrounding it were the momentum and horizontal angle hodoscopes. S4 was behind the Čerenkov counter, 256 in. from the quadrupole. To allow for multiple scattering, all trigger counters except S0 and the vertical dimension of S2 were made oversize. All trigger counters were constructed from Pilot *B* or *Y* scintillator and were 0.125 in. (S0), 0.25 in. (S1,S2), or 0.5 in. (S4) thick. For S1 and the vertical angle counters the usual magnetic shielding on the counter was insufficient. A large, soft iron plate was mounted just to the rear of the quadrupoles to give additional magnetic shielding. A 5-by-9-in. hole was cut to allow the particles to pass through. The acceptance defined by the basic fourfold coincidence was 35 mrad in vertical angle and 20 mrad in horizontal angle, yielding a solid angle per arm of 7×10^{-4} sr. The momentum acceptance was 14.3% (full

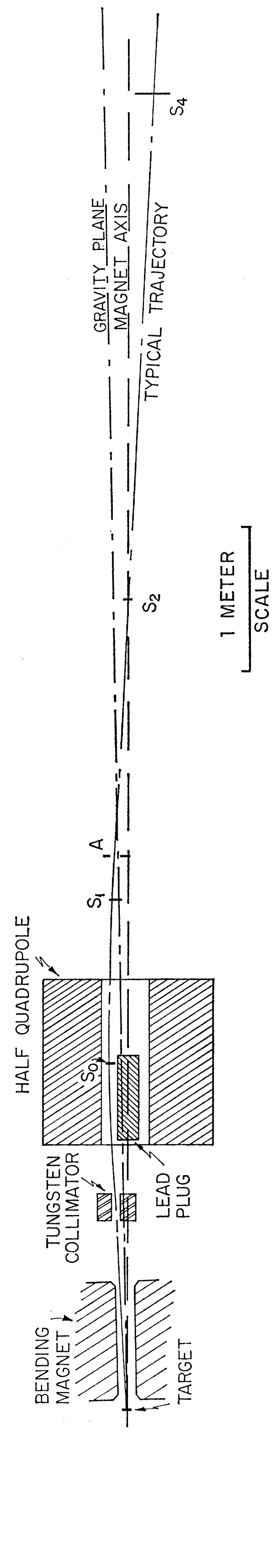

FIG. 7. Vertical cross section through the apparatus showing to scale the bending magnet, the tungsten collimator, the half-quadrupole magnet, and the positions of the scintillation counters S0, S1, A, S2, and S4.

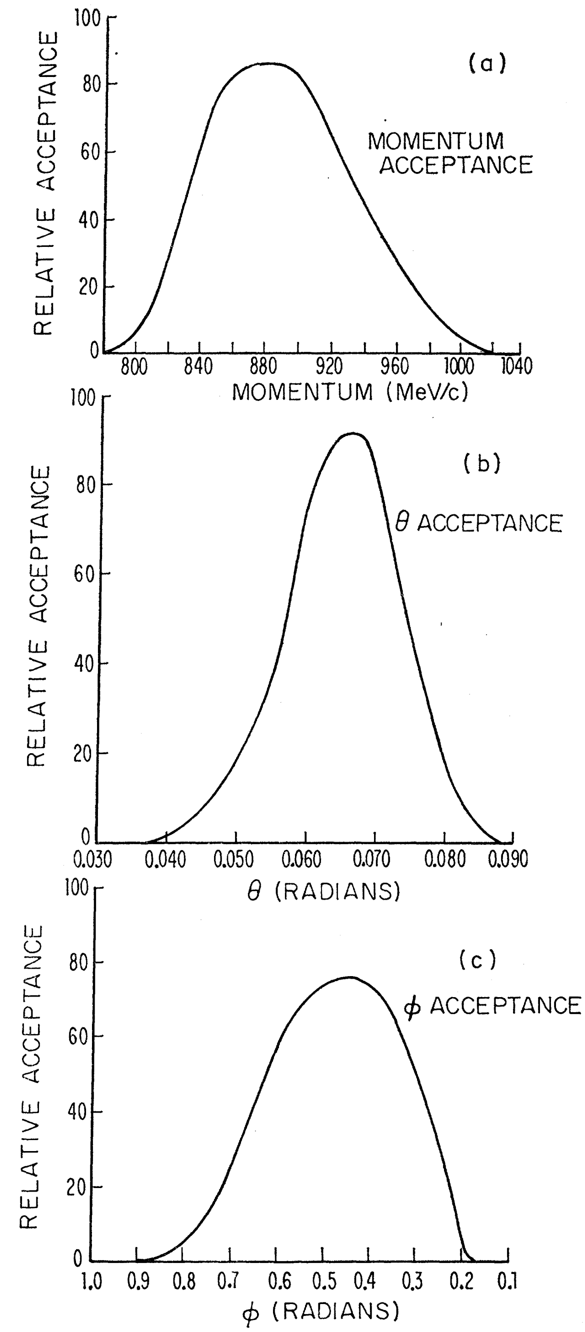

FIG. 8. Plots showing the relative acceptance of the apparatus for the point with a nominal momentum of 0.9 GeV/c and a nominal pair half-angle of 3.5°.

width at half-maximum). Figure 8 shows the acceptance of one spectrometer arm in p, θ, and φ.

The basic pair coincidence consisted of S0, S1, S2, S4, and the Čerenkov counter on each arm. This pair coincidence was referred to as $(VC)^2$. A pair coincidence omitting each S0 was referred to as $(TC)^2$. This coincidence was analogous to that of the first Harvard experiment.[7] The horizontal and vertical acceptance for $(TC)^2$ was defined by the tungsten collimator and the interior of the quadrupole.

To check for substantial showering behind the quadrupoles and to aid in the $(TC)^2$ aperture definition, an anticoincidence counter was located behind S1. This counter had a rectangular hole within a rectangular scintillator. The anticoincidence counter vetoed fewer than $(3.5\pm3)\%$ of the $(VC)^2$ pairs. The fraction of the $(VC)^2$ pairs vetoed at a momentum of 2.25 GeV/c was within 2% the same as the fraction vetoed at a momentum of 0.9 GeV/c.

The hodoscope counters provided the primary data for the asymmetric portion of the experiment. For symmetric pairs they gave a check of the distribution of particles across the aperture. Figure 9 shows the results of one such test.

E. Čerenkov and Shower Counters

A large, gas threshold Čerenkov counter was used to reject all particles except electrons and positrons. The counter was the same as used in the first Harvard experiment with somewhat less stringent optical requirements. The forward light was reflected by a parabolic mirror into a reflecting cone surrounding a 58-AVP photomultiplier. For alignment purposes a light source simulating Čerenkov light was moved over the range of incident particle trajectories. The Čerenkov counter was filled with freon-C318 at 8 psia.

A large shower counter followed S4. It consisted of alternating layers of 1 r.l. of lead, 1 in. of Plexiglas UVT Lucite, 1 r.l. of lead, and 0.5 in. of Pilot Y scintillator. The first Lucite occurred after 1 r.l. of lead plus 1 r.l. of steel due to the rear wall of the Čerenkov counter. A total of 8 r.l. of lead were used. The outputs from the four Lucite elements and from the four scintillator elements were each added to yield a "Lucite shower counter" and a "scintillator shower counter" signal. The Lucite shower counter gave better pion rejection, while thes cintillator shower counter gave better energy resolution.

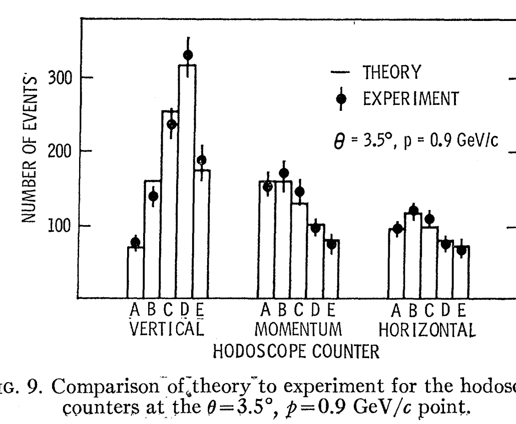

FIG. 9. Comparison of theory to experiment for the hodoscope counters at the $\theta=3.5°$, $p=0.9$ GeV/c point.

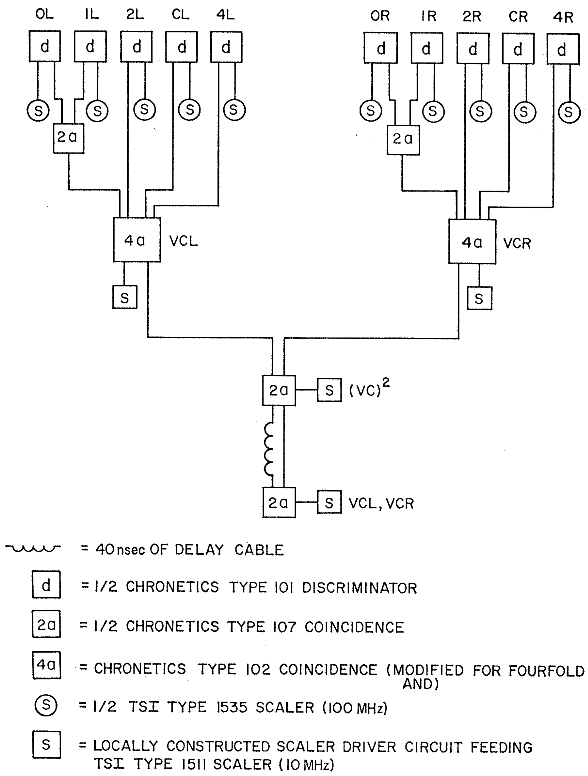

FIG. 10. Diagram of the electronics used for the major pair coincidence $(VC)^2$.

The shower counter efficiency was obtained by calibrating the counters on electrons and pions. The shower counters were used to check that particles producing a Čerenkov counter pulse also produced a large electromagnetic shower. The results of this test indicated that more than 98% of the pairs firing the Čerenkov counters were valid electron pairs.

F. Trigger Electronics

All counting electronics were located above the accelerator ring approximately 130 ft from the experimental apparatus. The trigger electronics were assembled from commercial circuits manufactured by Chronetics Inc. The primary $(VC)^2$ coincidence consisted entirely of these circuits. The secondary pair coincidences were formed from a combination of Chronetics circuits and locally constructed fanouts. The basic coincidences were duplicated using EGG equipment.

Figure 10 shows a block diagram of the primary electron-pair coincidence $(VC)^2$. Figure 11 shows a block diagram of the formation of the secondary electron-pair coincidences $(QC)^2$ and $(TC)^2$. $(QC)^2$ was the normal pair coincidence using alternate circuitry with a different random coincidence structure. The two types of rates agreed within the accuracy of the random coincidence corrections.

G. Recording Electronics

In addition to the trigger electronics substantial circuitry was devoted to recording up to 144 bits per event. Figure 12 shows a block diagram of the recording electronics. Further details have been given elsewhere.[26]

The time-to-amplitude converter circuits (TAC) were used to provide precise arm-to-arm timing with 1.5-nsec resolution (full width at high-maximum). This figure may be compared with the 8.7-nsec resolution of the primary $(VC)^2$ coincidence. The two counters selected for this purpose were characterized by small time slew due to counter size (S0 and S1 rather than S2 or S4). A TAC coincidence was also formed between VCL and VCR to provide an over-all check of the $(VC)^2$ coincidence. Other pair randoms were studied by rotating the definition of the pair trigger to give access to all lower-order random coincidences.

H. Quantameter, Faraday Cup, and Integrator

Monitoring of the photon beam was performed with a quantameter. The CEA quantameter is an enlarged version of the original designed by Wilson.[27] The quantameter used in this experiment was CEA quantameter Q1-F and was filled with a 90%-He–10%-N_2 mixture. The calibration constant was measured to be 2.82×10^{16} GeV/C. For electron scattering runs the

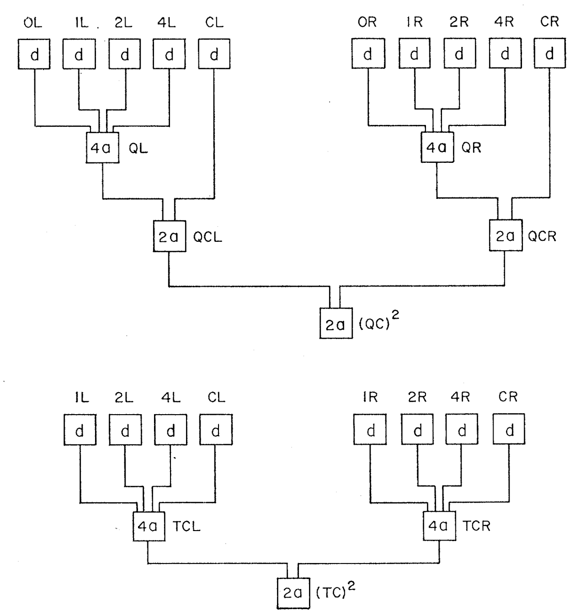

FIG. 11. Diagrams of the electronics for the auxiliary pair coincidences $(QC)^2$ and $(TC)^2$.

[27] For details concerning the CEA quantameters and their calibration see J. de Pagter and M. Fotino, Cambridge Electron Accelerator Report No. CEAL-1022, 1965 (unpublished); G. F. Dell and M. Fotino, Cambridge Electron Accelerator Report No. CEAL-1040, 1969 (unpublished).

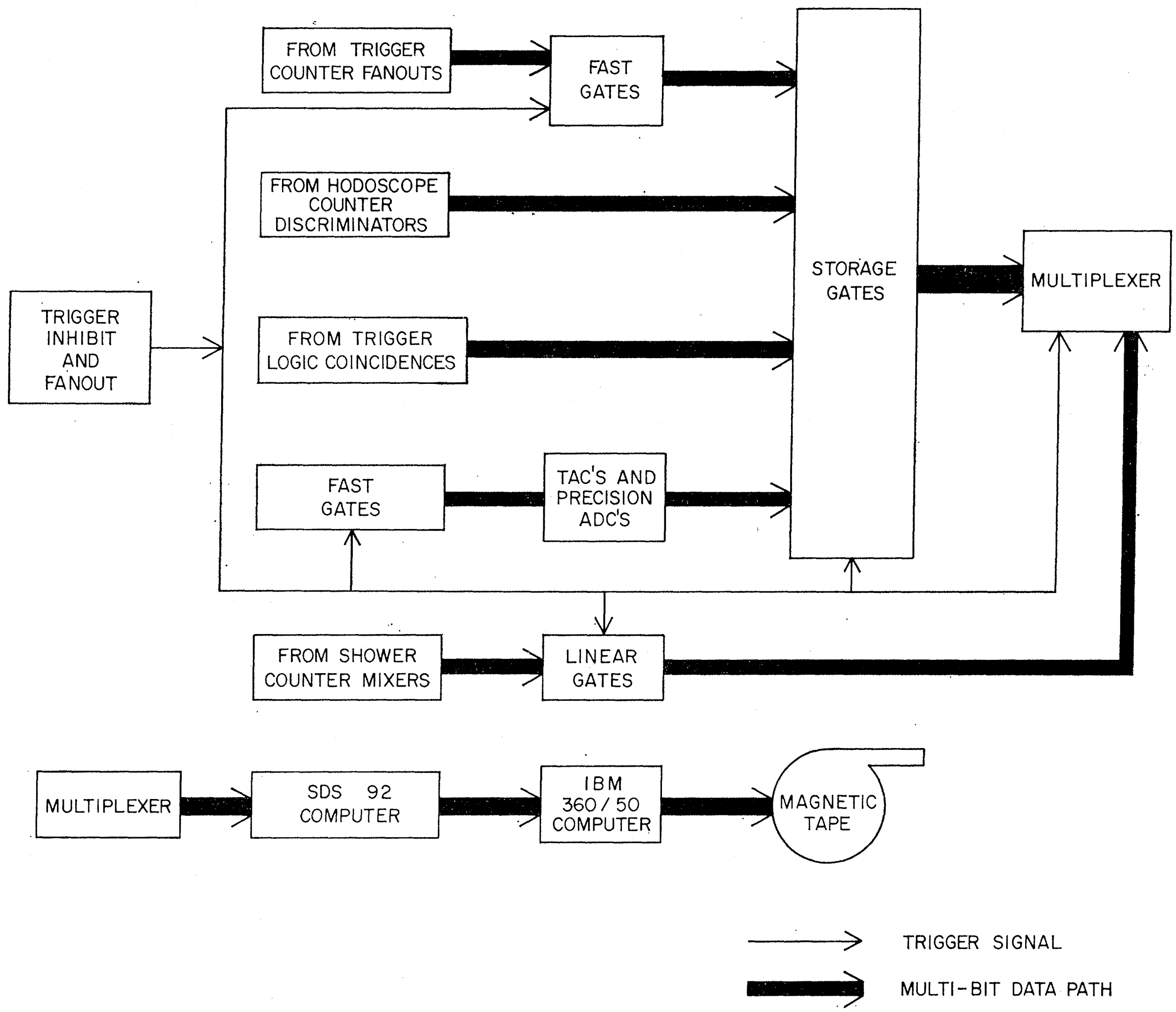

FIG. 12. Block diagram of the counter-computer system used to record auxiliary information such as counters not in the trigger, time-to-amplitude spectra, shower spectra, auxiliary coincidences, and hodoscope counters.

beam was monitored with a CEA Faraday cup. Both the quantameter and Faraday cup produced output currents such that the integrated charge was proportional to the total incident flux. The output currents of the quantameter or Faraday cup were used to charge a capacitor in a CEA-designed integrator.[28]

IV. EXPERIMENTAL PROBLEMS AND METHODS

A. Experimental Problems

Three problems associated with electron pair production influenced the design of the apparatus and the choice of running conditions. First, at large angles and energies the pion-pair flux can exceed the electron-pair flux by a factor greater than 100. Excellent pion rejection is required. Second, at small angles and energies the single-arm electron and positron rates become large. Their product increases faster than the pair rate. As a result the data-taking rate is limited by random coincidences. Because of the large absolute pair rate this limit is not a serious problem. Third, at large angles and energies the instantaneous rates in the counters limit the data-taking rate.

B. Counter Efficiencies and Timing

Subsequent to assembly each scintillation counter was checked with a Bi^{207} source or with cosmic rays. After the counters were mounted on the spectrometer arms they were carefully timed and plateaued. The relative timing of inputs to the coincidence circuits was checked using delay curves to an accuracy of 1 nsec. The internal timing of the electronics was done using a sampling scope to an accuracy of 0.5 nsec.

For a significant portion of the data a small in-

[28] L. A. Law and J. Weinstein, Cambridge Electron Accelerator Report No. CEAL-1021, 1965 (unpublished).

efficiency in one counter, S0L, remained undetected. It showed up during a final check of the plateauing efficiency at the end of the experiment. When replateaued with pion pairs the counter showed a $(5\pm2)\%$ inefficiency. The results from measurements of electron scattering confirmed this value. A check of the time dependence of the single-arm pion rates showed that there was no gradual deterioration. This correction was applied to all the pair rates.

C. Apparatus Alignment

Because of the character of the pair and single-arm cross sections, very small surveying errors could produce large changes in the counting rates. A 1% change in the effective spectrometer momentum could produce a 10% change in the single-arm and pair counting rates. The focusing of the spectrometer was such that a 0.100-in. change in the vertical position of S2 (0.130 in. for the target) was equivalent to a 1% change in momentum. The angular position of S0 was likewise critical. A 0.010 displacement of S0 produced a 0.3% change in horizontal angle yielding a 2% change in electron pair rates. The details of the alignment procedure are described elsewhere.[26]

The photon beam position was measured at the rear of the bending magnet using aluminum crosshairs and Polaroid or x-ray film. Exposures were also taken at the entrance to the quantameter hut. These pictures verified that the photon beam was centered in the quantameter and gave a measurement of the divergence of the beam.

D. Magnet Calibration

The calculated electron-pair rate depended strongly on the calibration of the magnets. The bending magnet coupled momentum and production angle such that a 1% error in the field of the bending magnet produced a 10% change in the pair counting rate; a 1% error in the field of one of the quadrupoles produced a 5% change in the pair counting rate. A nuclear-resonance probe was used to measure the magnetization curve of the bending magnet and a rotating-coil Rawson probe was used to study the profile of the field. A rotating-coil Rawson probe was used to measure the magnetization curves and the gradient of the half-quadrupole magnets. The errors in the magnetization curves are estimated to be 0.1%. The magnetization curve for the bending magnet deviated from linear by less than 1% at 12.8 kG (2.25 GeV/c particles).

For the bending magnet, an effective length L was determined by long-coil, Rawson-probe, and electron-beam measurements. The effective length was corrected for three effects. First, the target was located within the upstream fringe field. Second, the bending magnet lacked cylindrical symmetry and there was an azimuthal dependence of the effective length. Third, the magnetic center did not correspond to the geometric center of the bending magnet but was located 0.4 in. upstream. The estimated over-all error in the effective length is $\pm0.5\%$. A change in L as a function of current would produce an apparent momentum dependence of the electron-pair rate. Two separate upper limits on this effect were obtained. An integration of the Rawson-probe measurements yielded $\Delta L/L=0.23\%$ between 9.5 and 13.5 kG. The long-coil measurements yielded $\Delta L/L=0.1\%$ between 8.0 and 13.5 kG.

The quadrupole effective length was obtained from elastic electron scattering. The measured peak location determined the product of the quadrupole gradient and length to 0.25%. The quadrupoles were far from saturation, and a current-independent calibration constant was used. The results of the long-coil measurements yielded a limit on the current-dependent error of 0.25%.

The electron-pair counting rates were calculated by ray tracing using first-order magnet optics. For the bending magnet the nominal ray was determined by a stepwise integration through the field. Radial distributions from the Rawson-probe measurements were used. The values in the fringe-field region were corrected for the three effects cited above.

TABLE II. Ratio of experiment to theory for the two thickness targets used at the $\theta=3.5°$, $p=0.9$ GeV/c point. The error is the statistical error and does not take into account possible systematic errors.

Target thickness (in.)	Ratio of experiment to theory
0.25	1.08 ± 0.06
0.5	1.08 ± 0.05

E. Target-Thickness Dependence

The bulk of the electron-pair data was taken with an 0.5-in.-thick carbon target. One set of runs at $\theta=3.5°$, $p=0.9$ GeV/c was taken with a 0.25-in. carbon target. The real-photon and virtual-photon radiative corrections were independent of target thickness. The ratios of experiment to theory obtained for the two target thicknesses are summarized in Table II.

F. Electron Scattering

Electron scattering was used to give an independent check on the acceptance of the spectrometer.[19] During this experiment and a subsequent experiment, measurements were made of the electron scattering from carbon at incident electron energies from 1 to 4 GeV. The area of the quasi-elastic peak was then compared with the calculated cross section for scattering from carbon. The average ratio of experiment to theory was 0.97 ± 0.05. These measurements also confirmed the 5% plateauing inefficiency for the left arm. Since the bending magnet was not used during the electron scattering, these measurements do not rule out systematic errors due to the bending magnet.

V. RATE CALCULATIONS AND CORRECTIONS

A. Dead Times

The trigger counters operated at instantaneous rates up to several megahertz. An extensive study of the dead time of the discriminators was made and the data were corrected for dead time. The dead-time correction to the pair coincidence $(VC)^2$ was in all cases less than 5%.

B. Random Coincidences

Two types of random coincidences contributed significantly to the $(VC)^2$ rate. At low energy, and especially at the lower angle, random coincidences between a real electron and a real positron were large. For all but the earliest data these random coincidences were kept below 10% of the $(VC)^2$ rate. We will refer to these as fivefold randoms. A second random coincidence involved a real electron pair passing through nine of the counters entering $(VC)^2$ with an uncorrelated background particle in the tenth counter. This random coincidence was less than 4% at all points. We will refer to these as ninefold randoms. They were dominated by an off-momentum pair in coincidence with a background particle in S2.

The fivefold random coincidence rate was checked by three separate methods. The first involved calculating the random coincidence rate knowing its single-particle components and the resolving time of the coincidence circuits. The second method consisted of scaling the fivefold random directly. The third method used the TAC circuitry to study the $(VC)^2$ coincidence with a resolving time of 3.0 nsec. For the ninefold randoms the computer gave all of the real-particle ninefold rates provided that no single counter was always in the computer trigger. All single-counter rates were scaled to yield the necessary singles rates. Figure 13 shows a typical $(1)^2$ TAC spectrum at $\theta=3.5°$, $p=0.9$ GeV/c. The calculated random coincidence rate (from its components) was 9%, with negligible statistical error. At this point the scaled random rate was $9\pm2\%$, and the TAC spectrum yielded $9\pm2\%$.

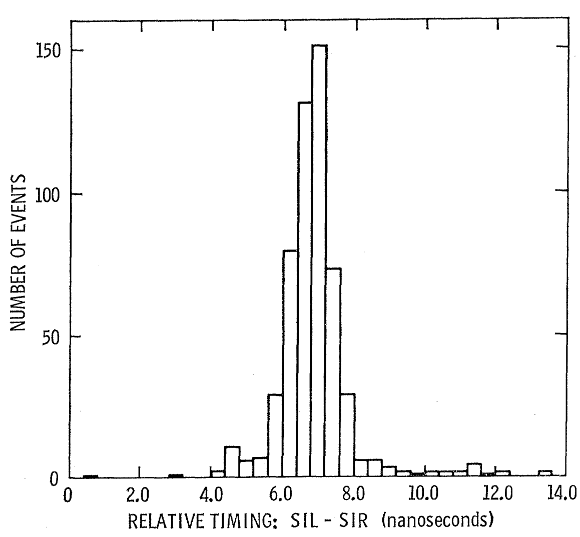

FIG. 13. Plot of the time-to-height spectrum for S1R relative to S1L. This spectrum can be further reduced in width by using the information from the hodoscope counters to correct for the size of the scintillation counter.

TABLE III. Ratio of the pion-pair rate to the electron-pair rate for the four points at which data were taken.

Momentum of one member of pair (GeV/c)	Angle between one member of pair and photon beam (Deg.)	Ratio of pion-pair rate to electron-pair rate
0.9	3.4	0.03
0.9	5.8	0.84
2.25	3.4	0.4
2.25	5.8	173.0

C. Target-Out Rates

The use of a vacuum beam path from the bremsstrahlung radiator to the downstream edge of the bending magnet kept the pair target-out rates small. The major source of target-out pairs was the 0.0015-in. aluminum window located 8 in. upstream of the carbon target. Using only the low-energy data, we obtained $(1.0\pm0.5)\%$ as the observed target-out rate. For the high-energy points, there were no target-out electron-pair events. The pion-pair target-out rate was 0.25% at $\theta=5.8°$, $p=2.25$ GeV/c.

D. Pion Contamination

The primary background of real particles was pions. Table III gives the observed ratio of pions to electrons for the four regions in which data were taken. The Čerenkov counter was used to eliminate the background flux of pions, and the shower counters were used to confirm the rejection.

The computer data permitted a determination of the pion contamination. With the computer triggered on any particle pair, we obtained the ratio of electron-positron–to–electron-pion (or positron-pion) coincidences. Since no first-order process allows the photoproduction of an electron-pion pair, the ratio is a measure of the contamination. The contamination is due to the inefficiency of the Čerenkov counter plus knock-on electrons produced by pion pairs. Experimentally we obtained for the fraction of pions simulating an electron

$$\begin{aligned}\text{left arm:}\quad &(0.36\pm0.09)\times10^{-2},\\ \text{right arm:}\quad &(1.05\pm0.10)\times10^{-2},\\ \text{pairs:}\quad &(0.38\pm0.10)\times10^{-4}.\end{aligned}$$

TABLE IV. Thickness of elements upstream of S2 which contribute to multiple scattering and bremsstrahlung.

Element	Length	Length (r.l.)
0.5-in. C tgt	2.1573 g/cm^2	0.0254
0.25-in. C tgt	1.091 g/cm^2	0.0128
Stainless steel vac. chamber window	0.002 in.	0.0026
Air before quadrupole	∼25 in.	0.0022
S0	0.125 in.	0.0077
S1+2 vert. ctrs.	0.375 in.	0.0230
Air after quadrupole	108 in.	0.0096
Air in quadrupole	52 in.	0.0046

TABLE V. Calculated correction due to multiple scattering for the four points at which extensive data were taken.

Momentum of one member of pair p_{nom} (GeV/c)	Angle between one member of pair and photon beam θ_{nom} (Deg.)	Calculated multiple-scattering correction (%)
0.9	3.4	-6 ± 2
0.9	5.8	$+1\pm2$
2.25	3.4	-2 ± 1
2.25	5.8	0 ± 1

The determination was made at the high-energy high-angle point where the pion-to-electron ratio was largest. Allowing for the relative electron- and pion-pair rates the resulting contamination of electron pairs for this point was of the order of 1%. At all other data points, the pion-pair contamination was negligible.

E. Photon Spectrum

The number of photons per unit energy interval can be written in general form as

$$f(k,k_x)/k. \tag{24}$$

It is conventional to use the equation for the definition of an equivalent quantum to normalize $f(k,k_x)$. This equation is

$$\int_0^{k_x} k\frac{f(k,k_x)}{k}dk=k_x. \tag{25}$$

We used the thick-target bremsstrahlung spectrum given by Tsai and Whitis[29] and changed the normalization from per incident electron to per equivalent quantum. Radiator thicknesses of 0.1 and 0.2 r.l. were used. The cross sections given in the results are corrected to a radiator of infinitesimal thickness.

F. Multiple Scattering

The dominant multiple-scattering correction was due to the differential effect of particles scattering into and out of S0 and S2. In the ray tracing, multiple scattering was evaluated by simulating a random scattering each time the particle passed through a spectrometer element of finite thickness.

The usual simulation assumes a Gaussian distribution of half-width $\Delta\theta=(0.015/p)\sqrt{L}$, where p is the particle momentum (GeV/c) and L is the length of the scattering element in radiation lengths. Because of the rapid angular variation of the cross section, the tails of the multiple scattering distribution can have an anomalously large effect. Scott has given an improved version of the multiple-scattering distribution in the "plural scattering" region.[30] Since the distribution may be of use in other experiments we have collected together Scott's results in Apendix C. We used Scott's formulas in calculating our results. For our situation, Scott's formulas gave the same results as the more conventional Gaussian theory.

The change in angle was applied separately to the vertical and horizontal angles. Table IV gives the thickness in radiation lengths of the relevant elements of the spectrometer. The air upstream of and within the quadrupoles was treated by formulas for multiple scattering from an extended scatterer within a magnetic field. The air between the counters downstream of the quadrupole was treated using the formulas given by Rossi.[31] The calculated corrections to the theoretical rate due to multiple scattering are summarized in Table V.

G. Bremsstrahlung Loss

Bremsstrahlung in the target and along the arm implies that the incident photon energy exceeds the sum of the final momenta. The effect for electron pairs is to decrease the theoretical counting rate. Bremsstrahlung in the target may be calculated in two ways. One method is to treat it as a radiative correction similar to the real-photon radiative correction (see Sec. II). The alternative method is to treat it by random tossing during the ray tracing. We used both methods; the two calculations were in good agreement. Bremsstrahlung along the arm can be treated only by ray tracing. We must consider all elements before the downstream end of the quadrupole. Beyond the quadrupole a change in momentum has no effect on the particle acceptance.

The bremsstrahlung correction is independent of the absolute energy and depends on the fractional energy acceptance. The effect, excluding the target contribution, was evaluated at $\theta=5.8°$, $p=0.9$ GeV/c and was found to yield a decrease in the theoretical pair rate of (8.0 ± 2.0)%. This effect was calculated at $\theta=3.5°$ and the 5.8° results agreed within the statistical error of the calculation.

Another bremsstrahlung correction was considered. A particle passing through the rear wall of the Čerenkov

[29] Y. S. Tsai and V. Whitis, Phys. Rev. **149**, 1248 (1966).
[30] W. T. Scott, Rev. Mod. Phys. **35**, 231 (1963).
[31] B. Rossi, *High-Energy Particles* (Prentice-Hall, Englewood Cliffs, N. J., 1952).

TABLE VI. Summary of the experimental rates and the corrections. One click equals 2.82×10^{11} GeV of integrated energy in the photon beam. The correction for the S0L plateau and the target out was the same for all data points. The s and a after the p_{nom} indicate symmetric points for which the two arm momenta were equal and asymmetric points for which the central momentum of one arm was higher by 4% than the nominal momentum and the central momentum of the other arm was lower by 4% than the central momentum.

θ_{nom} (deg)	p_{nom} (GeV/c)	Polarity	Dead time (%)	Fivefold randoms (%)	Ninefold randoms (%)	Finite conv. (%)	Pion contam. (%)	S0L plateau (%)	Target out (%)	Net rate (counts/click)	Statistical error (counts/click)
3.3	0.90s	nor	+0.7	−18.3	0	+3.0	···	+5.0	−1.0	3.738	0.158
		rev	+0.9	−19.3	0	+3.0				3.958	0.178
3.3	2.25s	nor	+1.4	−2.8	−1.2	+6.0	···			0.2767	0.0131
		rev	+1.4	−2.3	−1.0	+6.0				0.3055	0.0137
3.5	0.90s	nor	+0.6	−9.3	0	+6.0	···			2.345	0.142
		rev	+0.6	−8.4	0.1	+6.0				2.268	0.140
3.5	2.25s	nor	+1.8	−1.5	−2.8	+5.0	···			0.1596	0.0089
		rev	+2.0	−1.6	−2.8	+6.0				0.1844	0.0099
5.8	0.90s	nor	+3.2	−8.4	−3.3	+6.0	···			0.1125	0.0078
		rev	+4.3	−8.7	−3.4	+6.0				0.1183	0.0078
5.8	2.25s	nor	+3.9	−1.3	−4.2	+6.0	−1.0			0.007655	0.000630
		rev	+4.0	−1.5	−4.9	+6.0	−1.0			0.006926	0.000630
5.8	0.90a	nor	+3.6	−12.2	−6.0	+6.0	···			0.0994	0.0075
		rev	+3.9	−12.3	−6.0	+6.0	···			0.1112	0.0082
5.8	2.25a	nor	+2.0	−1.5	−4.8	+6.0	−1.0			0.006026	0.000540
		rev	+3.3	−1.4	−4.2	+6.0	−1.0			0.006988	0.000600

TABLE VII. Summary of the theoretical rates and the corrections to the theoretical rates. One click equals 2.82×10^{11} GeV of integrated energy in the photon beam. The theoretical rate was calculated using the approximate form of the cross section; the error introduced is less than 1%. The arm bremsstrahlung correction was the same for all data points. The s and a after the p_{nom} indicate symmetric points for which the two arm momenta were equal and asymmetric points for which the central momentum of one arm was higher by 4% than the nominal momentum and the central momentum of the other arm was lower by 4% than the nominal momentum.

θ_{nom} (deg.)	p_{nom} (GeV/c)	Beam atten. and rad. corr. (%)	Target brems. (%)	Mult. scatt. (%)	Arm brems. (%)	Čerenkov tank brems. (%)	Net rate (counts/click)
3.3	0.90s	−3	−13	−6±2	−8±2	−4.0	3.884
	2.25s	−4	−13	−2±1		−1.5	0.2586
3.5	0.90s	−3	−13	−6±2		−4.0	2.2588
	2.25s	−4	−13	−2±1		−1.5	0.1520
5.8	0.90s	−4	−13	+1±1		−4.0	0.1187
	2.25s	−5	−13	−0±1		−1.5	0.007122
5.8	0.90a	−4	−12	+1±1		−4.0	0.1014
	2.25a	−4	−12	−0±1		−1.5	0.005833

TABLE VIII. Summary of the ratios of theory to experiment for the various data points. The ⟨ ⟩ indicate averages over the acceptance of the apparatus. The expression e.q. is an abbreviation for equivalent quantum.

θ_{nom} (deg.)	p_{nom} (GeV/c)	$\langle\theta\rangle$ (deg.)	$\langle p\rangle$ (GeV/c)	$\langle -q^2\rangle^{1/2}$ (MeV/c)	$\langle Q_M{}^2\rangle^{1/2}$ (MeV/c^2)	R (expt/theory)	Statistical error	$d\sigma/d\Omega^2dp^2$e.q. (μb/sr^2 GeV^2 e.q.)
3.3	0.90s	3.23	0.846	11.1	97.4	1.083	3.1	107560
	2.25s	3.23	2.117	27.0	243.4	1.198	3.4	2968.9
3.5	0.90s	3.50	0.878	12.1	109.4	1.083	4.5	61338
	2.25s	3.50	2.196	29.4	272.6	1.161	3.3	1650.3
5.8	0.90s	5.72	0.880	18.9	177.9	1.002	5.0	2741
	2.25s	5.72	2.202	45.9	443.7	1.076	6.2	69.79
5.8	0.90a	5.70	0.877	21.9	177.3	1.035	5.5	2406
	2.25a	5.72	2.203	52.4	444.6	1.150	6.4	61.21

TABLE IX. Summary of the results for $(\text{TC})^2$. The arm bremsstrahlung was taken to be the same for both points. The total error consists of the statistical error and an estimate of the systematic error added in quadrature.

θ_{nom} (deg.)	p_{nom} (GeV/c)	Fivefold randoms (%)	Experimental rate (counts/click)	Mult. scatt. (%)	Arm brems. (%)	Theoretical rate (counts/click)	R (expt/theory)	Total error (%)
3.5	0.90s	16	3.42 ±0.13	−9±5	−15±4	3.03	1.13	8
3.5	2.25s	4	0.232±0.007	−3±2		0.208	1.12	7

TABLE X. A summary of the estimates of the momentum-dependent systematic errors. These errors could change the ratio of experiment to theory for the 0.9 and 2.25 GeV/c nominal momenta in a different way.

Item	Estimated error in % 3.4°	5.8°
1. Random coincidences and dead times	1.5	1.0
2. Calculation of multiple scattering	4.0	2.0
3. Undetected saturation of magnets	2.0	2.0
4. Rejection of events due to anticoincidence counter	2.0	2.0
5. Rejection of additional events by shower counters	1.0	1.0
Total (combined in quadrature)	5.2	3.7

TABLE XI. Summary of the errors which would effect the over-all normalization of all the points in the same manner.

Item	Estimated error in %
1. Calibration of magnets	5.0
2. Surveying	2.5
3. Calculation of bremsstrahlung and multiple scattering	2.0
4. Error in Monte Carlo calculation of theoretical rate	1.5
5. Error in theoretical rate due to ray tracing	1.0
6. Calibration of quantameter	2.0
Total (combined in quadrature)	6.5

tank could undergo bremsstrahlung and lose enough energy so that it would not count in S4. We measured a 4.0% loss at low energies and a 1.5% loss at high energies. These measurements agreed with the calculated loss.

H. Rate Calculations

The experimental rate was obtained by correcting the scaler data for dead times, random coincidences, pion contamination, target out, and counter inefficiencies. The theoretical rate was calculated by a Monte Carlo integration of the cross section over the acceptance of the apparatus. The Monte Carlo program took into account both multiple scattering and bremsstrahlung along the arm. The intensity of the photon beam was assumed to be uniform and the angular divergence of the beam was neglected.

VI. RESULTS AND CONCLUSIONS

A. Electron-Pair Results

The results are presented in terms of eight data points labeled by the nominal half-angle, the nominal lepton momentum, and whether the quadrupole currents were equal or 4% asymmetric. For each point, data were taken with both polarities for the magnets.

The experimental results for the electron-pair coincidence $(VC)^2$ are summarized in Table VI. This table gives the results for each data point and each polarity. Weighted averages for all corrections are tabulated. There is no statistically significant polarity dependence of the electron-pair rates. Table VII gives the corresponding theoretical rates and corrections. Table VIII gives the ratios of experiment to theory and the error due to counting statistics. The differential cross section corresponding to the experimental rate is also given. The $(TC)^2$ results are summarized in Table IX.

There are two types of systematic errors which are relevant to the interpretation of the result: those which can give a momentum dependence at fixed angle and those which can give a correction to the over-all normalization. Table X gives an estimate of the momentum-dependent systematic errors; Table XI gives an estimate of the normalization errors.

Both the $(VC)^2$ and $(TC)^2$ results agree with the predictions of quantum electrodynamics. Expressed as a function of $Q_M{}^2$, the mass of the electron-positron pair in $(\mathrm{MeV}/c^2)^2$, the ratio R of experiment to theory for $(VC)^2$ is

$$R=(1.09\pm0.02)[1+(31.6_{-41.2}^{+31.2})\times10^{-8}Q_M{}^2]. \quad (26)$$

The momentum-dependent systematic error $({}_{-32.4}^{+18.8})$ and the statistical error (±24.8) have been combined to obtain a total error in the coefficient of $Q_M{}^2$. The error in the normalization includes only the statistical error. There is an additional systematic normalization error of 6.5%. Only random coincidences, dead times, and multiple scattering represent actual corrections to the data. The other contributions represent possible undetected systematic errors and an estimate of their magnitude. In estimating our total momentum-dependent systematic error we have combined all of these errors in quadrature. The resulting error has been offset by half the value of the uncertainty of the magnetic field due to saturation to allow for the asymmetry of this correction.

This result can be compared with the results of the other experiments on electron pair production. They are

(1) Previous Harvard experiment,[7]

$$R=(0.94\pm0.02)[1+(513\pm38)\times10^{-8}Q_M{}^2]; \quad (27)$$

(2) DESY-MIT experiment,[11]

$$R=(0.94\pm0.02)[1-(5.5\pm14.8)\times10^{-8}Q_M{}^2]; \quad (28)$$

(3) MIT-CEA experiment,[12]

$$R=(1.12\pm0.27)[1-(87.8\pm145)\times10^{-8}Q_M{}^2]; \quad (29)$$

(4) Cornell experiment,[9]

$$R=(0.92\pm0.05)[1+(157\pm85)\times10^{-8}Q_M{}^2]; \quad (30)$$

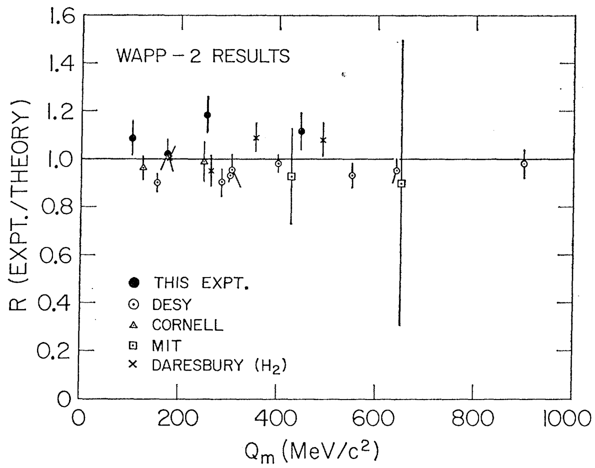

FIG. 14. Plot of the ratio of experiment to theory for representative points from all the recent electron-pair experiments which have been used to test QED. In all cases the errors are the statistical errors and do not include systematic errors.

(5) Daresbury hydrogen data,[13]

$$R=(1.024\pm0.028)+(1.31\pm1.31)\times10^{-12}Q_M{}^4;\quad (31)$$

(6) Daresbury carbon data,[13]

$$R=(1.042\pm0.020)-(1.04\pm0.91)\times10^{-12}Q_M{}^2.\quad (32)$$

For each of these experiments the error in normalization is the statistical error and it does not include the systematic errors. Figure 14 shows on one graph the ratio of theory to experiment for representative points from each of the major experiments.

Kroll has studied the simplest modification of quantum electrodynamics that could play a role in electron-positron pair production.[32] He showed that a modification consistent with the general principles of field theory could at the most lead to a fractional correction of the form $(Q_F/\Lambda)^4$. Here Q_F is the mass of the virtual lepton in the Feynman diagram for the photoproduction of symmetrical electron-positron pairs and Λ is the cutoff mass introduced by the modification of the theory. Since Kroll's work, several authors have treated the agreement between theory and experiment for pair production in terms of a parametrization of this form. Table XII summarizes the values of Λ obtained when the ratio of experiment to theory is parametrized in terms of the equation

$$R=A(1+Q_M{}^4/\Lambda^4).\quad (33)$$

TABLE XII. Limits on the cutoff parameter Λ for a deviation of the form $R=A(1+Q_M{}^4/\Lambda^4)$ for the three best experiments using wide-angle electron pairs as a test of quantum electrodynamics. The Daresbury data is for electron pair production from hydrogen.

Experiment	95% confidence limit
DESY-MIT	$\Lambda>1.4$ GeV/c^2
Daresbury	$\Lambda>0.7$ GeV/c^2
This experiment	$\Lambda>0.8$ GeV/c^2

[32] N. M. Kroll, Nuovo Cimento **45**, A65 (1966).

B. Conclusions

The results of this experiment verify the predictions of quantum electrodynamics in the invariant-mass range 97–445 MeV/c^2.

ACKNOWLEDGMENTS

We wish to acknowledge the support and encouragement of the director and the staff of the Cambridge Electron Accelerator throughout the course of this experiment. We also wish to thank the staff of the Harvard Cyclotron Laboratory for their support. Dr. R. Blumenthal supervised the general design of the new spectrometer arms and the air support system; he also contributed to the running in the early stages of the experiment. E. Sadowski did all the mechanical design work. B. Farmer, A. Sansone, and B. Sansone helped with the assembly and testing of the apparatus. R. Fessel made a major contribution to the SDS-92 and IBM 360 programs required to handle the counter bits; M. Fotino and F. Dell provided us with well-understood, calibrated quantameters and Faraday cups. Other members of our group who contributed significantly to the success of the experiment are B. Huld, L. Litt, N. Hicks, K. Stanfield, and V. Montana.

APPENDIX A: REDUCTION OF ELECTRON-PAIR CROSS SECTION

We will use the metric $p_1\cdot p_2=E_1E_2-\mathbf{p}_1\cdot\mathbf{p}_2$, where p_1, p_2 are arbitrary four-vectors; E_1, E_2 are the timelike components; and $\mathbf{p}_1$, $\mathbf{p}_2$ are the spacelike components. We use the expansion variables defined in the text. Under the assumption of near symmetric forward pairs, we may calculate $k\cdot p_+$, $k\cdot p_-$, and $p_+\cdot p_-$. Neglecting m^2, we have

$$k\cdot p_\pm=E^2\theta^2(1\pm e\pm2a+2ae+a^2-\tfrac{1}{12}\theta^2),\quad (A1)$$

$$p_+\cdot p_-=2E^2\theta^2(1-e^2-\tfrac{1}{3}\theta^2-\tfrac{1}{4}\varphi^2).\quad (A2)$$

Note that $\varphi\sim0$ (not $\varphi\sim\pi$) is implicit in the choice of sign for the φ^2 term. By directly using the relation

$$q^2=-2k\cdot p_+-2k\cdot p_-+2p_+\cdot p_-,\quad (A3)$$

we find

$$q^2=-4E^2\theta^2[(a+e)^2+\tfrac{1}{4}\varphi^2+\tfrac{1}{4}\theta^2].\quad (A4)$$

Expressed in terms of u, Eq. (A4) becomes

$$q^2=-4E^2\theta^2(u^2+\tfrac{1}{4}\theta^2).\quad (A5)$$

Note that $(q^2)_{\min}=-E^2\theta^4$ when $u^2=0$.

The DW calculation is performed using the general form factors $W_1(q^2,q\cdot p_i)$ and $W_2(q^2,q\cdot p_i)$. In keeping with our results on the carbon form factor we specialize to the case of elastic scattering from a spin-0 nucleus.

Then DW give

$$W_1=0, \tag{A6}$$

$$W_2=F^2(q^2)(M^2/E_f)\delta(E_i-E_f-q_0). \tag{A7}$$

If we integrate over the δ function and note that $E_f\approx M$, we obtain $W_2=F^2M$. After the integration over the incident photon spectrum, the DW cross section may be written

$$d\sigma_{\mathrm{DW}}=\frac{\alpha^3}{4\pi^2}\frac{d^3p_+}{E_+}\frac{d^3p_-}{E_-}\frac{f}{k}\frac{1}{q^4}W_{\mu\nu}M_{\mu\nu}\frac{1}{kM}. \tag{A8}$$

Here

$$W_{\mu\nu}M_{\mu\nu}=\frac{4}{x_1x_2}[-(x_6-x_5^2)(x_1+x_2+x_6) -\tfrac{1}{2}(x_1^2+x_2^2)+x_3x_5(x_1+x_2) -x_4x_5(x_1-x_2)-x_3^2x_6-x_4^2x_6]W_2. \tag{A9}$$

The integration over the photon spectrum also yields the photon energy. It is approximated by

$$k=2E[1+(E/M)\theta^2(u^2+\tfrac{1}{3}\theta^2)].$$

Now let us consider the case $k=4$ GeV, $E_+=E_-=2$ GeV, $\theta_+=\theta_-=0.1$, and $\varphi=0$. From DW we have the following definitions for the x's (elastic scattering):

$$x_2=2k\cdot p_-\approx E^2\theta^2\approx 0.08\ \ \mathrm{GeV}^2, \tag{A10}$$

$$x_2=2k\cdot p_+\approx E^2\theta^2\approx 0.08\ \mathrm{GeV}^2, \tag{A11}$$

$$x_3=k=4\ \mathrm{GeV}, \tag{A12}$$

$$x_4=E_--E_+\approx 0.2\ \mathrm{GeV}\ (\text{average over }15\%\ \text{momentum acceptance}), \tag{A13}$$

$$x_5=k-E_+-E_-\approx 0.004\ \mathrm{GeV}, \tag{A14}$$

$$x_6=q^2\approx -0.00016\ (\mathrm{GeV}/c)^2\ (\text{average over acceptance}). \tag{A15}$$

The approximate values come from evaluating the appropriate expansion. For x_4 and x_6 we have inserted averages over the pair acceptance. Equations (A10)–(A14) imply that we may neglect all terms containing x_5. Letting

$$2p_+\cdot p_-=x_1+x_2+x_6, \tag{A16}$$

we may rewrite $W_{\mu\nu}M_{\mu\nu}$ as

$$W_{\mu\nu}M_{\mu\nu}=(-2/k\cdot p_+k\cdot p_-)[(k\cdot p_+)^2+(k\cdot p_-)^2 +q^2(p_+\cdot p_-)+q^2(E_+^2+E_-^2)]W_2. \tag{A17}$$

This may be rewritten in the form

$$W_{\mu\nu}M_{\mu\nu}=2BW_2/k\cdot p_+k\cdot p_-,$$

where

$$B=-[(k\cdot p_+)^2+(k\cdot p_-)^2+q^2p_+\cdot p_-+q^2 \times(E_+^2+E_-^2)]. \tag{A18}$$

Consequently,

$$d\sigma_{\mathrm{DW}}=\frac{\alpha^3}{4\pi^2}\frac{d^3p_+}{E_+}\frac{d^3p_-}{E_-}\frac{f}{k}\frac{1}{q^4}\frac{2B}{k\cdot p_+k\cdot p_-}\frac{F^2}{k}. \tag{A19}$$

Near symmetry, there is implicit in B a two-orders-of-magnitude cancellation. If

$$q^2=-2k\cdot p_+-2k\cdot p_-+2p_+\cdot p_- \tag{A20}$$

is evaluated directly, one finds a second two-orders-of-magnitude cancellation. Numerically, these cancellations can lead to imprecise results with typical single-precision computer calculations. Finally, at exact symmetry there is one final level of cancellation which can easily lead to meaningless results.

APPENDIX B: FURTHER DISCUSSION OF FIRST HARVARD ELECTRON-PAIR EXPERIMENT

In this appendix we indicate some of the major changes in the apparatus, and discuss some of the suggestions for an explanation of the excess of electron pairs over that predicted by theory observed in the first Harvard electron-pair experiment. The current apparatus incorporated the following improvements over the apparatus used earlier[7]:

(1) The quadrupole apertures were moved closer to the median plane to enable the study of electron pairs with a smaller opening angle.

(2) 8-in.-long tungsten alloy collimators were placed after the bending magnet and just in front of the quadrupole magnets. The openings in these collimators did not define the acceptance.

(3) An additional trigger counter was added at the halfway point of the quadrupole. This counter was aperture defining.

(4) The obstacle in the center of the half-quadrupole magnets was shortened so that it ended 24 in. before the end of the quadrupole field.

(5) Hodoscopes were used to subdivide the acceptance in vertical angle, horizontal angle, and momentum.

(6) The previous electronics were replaced by commercial equipment with a smaller dead time and with a smaller resolving time.

(7) The counters were fed on line to a computer in such a manner that one could trigger the system on less than the full complement of trigger counters and measure all the contributions to the random coincidences.

(8) Time-to-pulse-height converters were incorporated so that one could obtain better resolving time.

(9) The shower counters were calibrated so that one obtained a direct check on pion rejection.

(10) The Čerenkov counter optics were simplified by using only one channel on each arm.

(11) The photon beam was produced from an external electron beam. This change permitted electron

scattering with the bending magnet off as a test of the spectrometer. It also allowed electron scattering to be used in calibrating the quadrupoles.

Most explanations for the excess of electron pairs observed in the first Harvard experiment[7] fall into the broad category of the leakage of particles through the quadrupoles. Two of the above changes had a direct effect on the leakage of particles. First, the collimator provided more matter between 0° electron pairs and the aperture. Specifically, it increased the attenuation of showers. Second, removal of the downstream portion of the lead obstacle eliminated a possible source of showers produced by low-momentum particles entering the quadrupole. If showering were a problem, these changes made the apparatus less sensitive to it. Because the two sets of apparatus were not directly comparable, we cannot prove that any of these effects were present in the first Harvard experiment, or if present, were the cause of the observed excess of electron pairs.

Another class of explanations of the observed excess was that some momentum-dependent correction had not been adequately allowed for. As a specific example, in the first experiment no estimate was available for anything but the arm-to-arm random coincidences. There is no evidence, however, from the present experiment that a significant class of random coincidences was omitted in the earlier experiment.

This second Harvard experiment is, however, superior to the earlier experiment and is regarded as proving that the first Harvard experiment was incorrect.

APPENDIX C: FORMULAS FOR CALCULATING CORRECTION DUE TO MULTIPLE SCATTERING

The normal first approximation to multiple scattering is to assume a Gaussian distribution of the form

$$f_g(\theta)=(2/\sqrt{\pi})\exp(-\theta^2). \qquad \text{(C1)}$$

Here θ is the reduced scattering angle where $\theta=\vartheta/\theta_g$, ϑ is the scattering angle in radians, and $\theta_g=(c_g/p)\sqrt{t}$. θ_g is the Gaussian scattering width (radians), c_g is a constant (0.015 GeV/c), p is the particle momentum (GeV/c), and t is the thickness of the scatterer (r.l.).

The Gaussian approximation fails because of the long tails characteristic of the underlying Coulomb scattering event. Many authors have studied this problem. Scott's article[30] contains a very general treatment of small-angle multiple scattering and further references. In this appendix we have collected together those portions of Scott's results needed to calculate small-angle multiple scattering in a somewhat better approximation than simple Gaussian. Specifically, we have followed Scott's use of a method due to Molière. All numbers in brackets refer to the equations in Scott's paper.

A. General Results

Scott's result is [7.49]

$$f_m(\theta,t)=\frac{2}{\sqrt{\pi}}\exp(-\theta^2)+\frac{1}{B}f^{(1)}(\theta)+\frac{1}{B^2}f^{(2)}(\theta)+\cdots. \qquad \text{(C2)}$$

The first term in Eq. (C2) is the usual Gaussian distribution with appropriate normalization. The higher-order terms are Molière's corrections. B is a number which is a complex function of the thickness of the scatterer. The angle θ is now the reduced scattering angle given by $\theta=\vartheta/\theta_m$. The Molière scattering width θ_m has the same functional form as θ_g; that is, $\theta_m=(c_m/p)\sqrt{t}$. The constant c_m, however, has a weak dependence on target thickness. Specifically,

$$c_m=B^{1/2}\pi m_e^2/\alpha\ln(183Z^{-1/3})$$
$$=4.85\times10^{-3}B^{1/2}, \qquad \text{(C3)}$$

where B (≈ 9) contains the target-thickness dependence, m_e is the electron mass, and Z is the atomic number of the scatterer. For typical scatterers with $Z=4$ and $B=9$, we find $c_m=0.014$ GeV/c, which is quite close to $c_g=0.015$ GeV/c. B is obtained as the solution of a transcendental equation and may be approximated by

$$B=1.153+2.583\log_{10}\Omega_0. \qquad \text{(C4)}$$

Ω_0 is the average number of scatterings undergone in passing through the scatterer. Scott gives it as the ratio of two angles, χ_c and χ_α. χ_c is characteristic of the total scattering angle for a scatterer of thickness t (in r.l.), and χ_α is characteristic of the scattering from a single totally screened atom. Using [7.38], viz.,

$$\Omega_0=\chi_c^2/\chi_\alpha^2, \qquad \text{(C5)}$$

we find

$$\Omega_0=\pi t/[\alpha\ln(183Z^{-1/3})][(1.0825)^2(1.13)^2\alpha^2Z^{2/3}], \qquad \text{(C6)}$$

where t is in r.l. For $Z=4$, $\Omega_0=4.46\times10^5t$.

The functions $f^{(n)}(\theta)$ are derived from certain hypergeometric functions. Specifically,

$$f^{(1)}(\theta)=(2/\pi)D_1(\tfrac{3}{2},\tfrac{1}{2},-\theta^2), \qquad \text{(C7)}$$

$$f^{(2)}(\theta)=(1/\pi)D_2(\tfrac{5}{2},\tfrac{1}{2},-\theta^2), \qquad \text{(C8)}$$

and D_1 and D_2 are tabulated in Table VIII of Scott's paper.

B. Detailed Derivation

In this section we relate the results for c_m and Ω_0 to the detailed expressions given by Scott. He defines the projected reduced scattering angle as [7.436]

$$\theta=\vartheta/\chi_cB^{1/2}, \qquad \text{(C9)}$$

where we have replaced Scott's ϕ, φ by the more usual θ, ϑ. The characteristic scattering angle is defined as

[7.4c]

$$\chi_c^2 = 4\pi e^4 z^2 Z(Z+1) N t / p^2 v^2, \qquad \text{(C10)}$$

where t is in cm. Here e is the electronic charge, z is the charge of the incident particle, Z is the charge of the scatterer, N is the number of scatterers per unit volume, p is the momentum of the incident particle, and v is the velocity of the incident particle. The units of χ_c are radians and the formula has actually been specialized to the case of incident electrons. Setting $z=1$ and replacing N by $N_0\rho/A$, where N_0 is Avogadro's number, ρ is the density of the scatterer (g/cm^3), and A is the atomic weight of the scatterer, we find

$$\chi_c^2 = \frac{4\pi e^4 Z(Z+1)(N_0\rho/A)t}{p^2 v^2}, \qquad \text{(C11)}$$

where t is in cm. For the definition of a radiation length we have[31]

$$\frac{1}{X_0} = 4\alpha \frac{N_0}{A} Z(Z+1) r_e^2 \ln(183 Z^{-1/3}), \qquad \text{(C12)}$$

where X_0 is expressed in g/cm^2, or

$$\frac{1}{X_0} = 4\alpha \frac{N_0\rho}{A} Z(Z+1) \frac{e^4}{m_e^2 c^4} \ln(183 Z^{-1/3}),$$

where X_0 is expressed in cm. Equation (C12) can be used to reexpress Eq. (C11) in the form

$$\chi_c^2 = \frac{\pi}{p^2 v^2} t \frac{m_e^2 c^2}{\alpha \ln(183 Z^{-1/3})}, \qquad \text{(C13)}$$

where t is in r.l. For very relativistic particles, $(v/c) \approx 1$. Expressing m_e in energy units we find

$$\chi_c^2 = \frac{\pi m_e^2}{\alpha \ln(183 Z^{-1/3})} t/p^2, \qquad \text{(C14)}$$

with t in r.l. Using our definition of θ_m, we have $\theta_m = \chi_c B^{1/2}$ or

$$\theta_m = B^{1/2} \left[\frac{\pi m_e^2}{\alpha \ln(183 Z^{-1/3})}\right]^{1/2} (t)^{1/2}/p, \qquad \text{(C15)}$$

with t in cm. This gives

$$c_m = B^{1/2} \left[\frac{\pi m_e^2}{\alpha \ln(183 Z^{-1/3})}\right]. \qquad \text{(C16)}$$

For Ω_0 we take Scott's definition of the characteristic scattering angle for complete screening [6.60a] and [6.96] with $c=1$:

$$\chi_\alpha = 1.0825 \chi_0, \qquad \text{(C17)}$$

where

$$\chi_0 = (1.13/137) Z^{1/3} (m_e/p). \qquad \text{(C18)}$$

Here the Born parameter $zZe^2/\hbar v$ has been assumed to be 0. Using Eq. (C14) for χ_c^2, we obtain

$$\Omega_0 = \chi_c^2 / \chi_\alpha^2, \qquad \text{(C19)}$$

or

$$\Omega_0 = \pi t / \alpha^3 \ln(183 Z^{-1/3}) (1.0825)^2 (1.13)^2 Z^{2/3}, \qquad \text{(C20)}$$

with t in r.l.